

This is the peer reviewed version of the following article:

Multiscale sensing of antibody-antigen interactions by organic transistors and single-molecule force spectroscopy / Casalini, Stefano; Dumitru, Andra C.; Leonardi, Francesca; Bortolotti, Carlo Augusto; Herruzo, Elena T.; Campana, Alessandra; De Oliveira, Rafael F.; Cramer, Tobias; Garcia, Ricardo; Biscarini, Fabio. - In: ACS NANO. - ISSN 1936-0851. - STAMPA. - 9:5(2015), pp. 5051-5062. [10.1021/acsnano.5b00136]

*Terms of use:*

The terms and conditions for the reuse of this version of the manuscript are specified in the publishing policy. For all terms of use and more information see the publisher's website.

28/04/2026 12:16

(Article begins on next page)

This document is confidential and is proprietary to the American Chemical Society and its authors. Do not copy or disclose without written permission. If you have received this item in error, notify the sender and delete all copies.

**Multi-scale sensing of antibody-antigen interactions by organic transistors and single molecule force spectroscopy**

Journal:	<i>ACS Nano</i>
Manuscript ID:	Draft
Manuscript Type:	Article
Date Submitted by the Author:	n/a
Complete List of Authors:	Casalini, Stefano; Università degli Studi di Modena e Reggio Emilia, Dipartimento di Scienze della Vita Dumitru, Andra; Instituto de Ciencia de Materiales de Madrid (CSIC), Leonardi, Francesca; Consiglio Nazionale delle Ricerche (CNR), Istituto per lo Studio dei Materiali Nanostrutturati (ISMN); Consiglio Nazionale delle Ricerche (CNR), Istituto per la Sintesi Organica e Fotoreattività Bortolotti, Carlo; Università degli Studi di Modena e Reggio Emilia, Dipartimento di Scienze della Vita Herruzo, Elena; Instituto de Ciencia de Materiales de Madrid (CSIC), Campana, Alessandra; Consiglio Nazionale delle Ricerche (CNR), Istituto per lo Studio dei Materiali Nanostrutturati (ISMN); "Alma Mater Studiorum"-Università di Bologna, Dipartimento di Chimica "G. Ciamician" de Oliveira, Rafael; São Paulo State University (UNESP) - Postgraduate Program in Materials Science and Technology, Cramer, Tobias; Consiglio Nazionale delle Ricerche (CNR), Istituto per lo Studio dei Materiali Nanostrutturati (ISMN); "Alma Mater Studiorum"-Università di Bologna, Dipartimento di Fisica e Astronomia Garcia, Ricardo; Instituto de Ciencia de Materiales de Madrid (CSIC), Biscarini, Fabio; Università degli Studi di Modena e Reggio Emilia, Dipartimento di Scienze della Vita

SCHOLARONE™  
Manuscripts

1  
2  
3  
4  
5  
6  
7  
8  
9  
10  
11  
12  
13  
14  
15  
16  
17  
18  
19  
20  
21  
22  
23  
24  
25  
26  
27  
28  
29  
30  
31  
32  
33  
34  
35  
36  
37  
38  
39  
40  
41  
42  
43  
44  
45  
46  
47  
48  
49  
50  
51  
52  
53  
54  
55  
56  
57  
58  
59  
60

# Multi-scale sensing of antibody-antigen interactions by organic transistors and single molecule force spectroscopy

*Stefano Casalini*<sup>1,\*</sup>, *Andra Dumitru*<sup>2</sup>, *Francesca Leonardi*<sup>3,4</sup>, *Carlo A. Bortolotti*<sup>1</sup>, *Elena T. Herruzo*<sup>2</sup>, *Alessandra Campana*<sup>5,3</sup>, *Rafael F. de Oliveira*<sup>1,6</sup>, *Tobias Cramer*<sup>3,7</sup>, *Ricardo Garcia*<sup>2,\*</sup>, *Fabio Biscarini*<sup>1,3</sup>

<sup>1</sup> Life Sciences Department, Università di Modena e Reggio Emilia, Via Campi 183, 41125 Modena, Italy.

<sup>2</sup> Instituto de Ciencia de Materiales de Madrid (CSIC), 28049 Madrid, Spain.

<sup>3</sup> *CNR-ISMN* Consiglio Nazionale delle Ricerche, Istituto per lo Studio dei Materiali Nanostrutturati, Via Gobetti 101, 40129 Bologna, Italy,

<sup>4</sup> *CNR-ISOF* Consiglio Nazionale delle Ricerche, Istituto per la Sintesi Organica e Fotoreattività, Via Gobetti 101, I-40129 Bologna, Italy.

<sup>5</sup> “Alma Mater Studiorum”-Università di Bologna, Dipartimento di Chimica “G. Ciamician”, Via Selmi 2, 40126 Bologna, Italy.

<sup>6</sup> São Paulo State University, Unesp, Postgraduate Program in Materials Science and Technology, 17033-360, Bauru, SP, Brazil

<sup>7</sup> “Alma Mater Studiorum”-Università di Bologna, Dipartimento di Fisica e Astronomia, Viale Berti Pichat 6/2, 40127, Italy.

KEYWORDS: organic field effect transistors, immunosensing, interleukin-4, force spectroscopy, atomic force microscopy, biorecognition, bioelectronics.

**ABSTRACT**

Antibody-antigen recognition in real label-free electronic biosensors is studied by a multi-scale approach combining measurements with an electrochemically-gated organic field-effect transistor (EGOFET) and single molecule force spectroscopy. Detection of anti-inflammatory cytokine, interleukin-4 (IL-4), down to 5 nM concentration is achieved using gate electrodes functionalized with IL-4 antibodies on different adhesion layers. Single force spectroscopy on the same electrodes reveals that (un-)binding force between IL-4 on the tip and its antibodies grafted onto the surface is distributed according to a chi-square distribution with mean force  $\approx 100$  pN and standard deviation  $\approx 57$  pN, independently on the adhesion layer used. Its positive skewness reflects the finite probability of multiple specific bonds between tip and surface. The control experiments (where specific binding is prevented either by the absence of the antibody or by a different antigen at the tip) yield significantly different distributions and absence of multiple binding events. The highest probability of specific binding (about 30%) is observed on Au electrodes functionalized with His-tagged protein G (PG), revealing that PG yields the largest areal density of oriented (thus available for recognition events) antibodies. The enhanced sensitivity observed in EGOFET functionalized with protein G lies in the strong electrostatic coupling of the highly oriented IL-4 antibodies with the charge carriers in the transistor channel.

## 1. INTRODUCTION

Immunosensing exploits one of nature's most optimized molecular recognition mechanisms, namely the interaction between an antigen (Ag) and its specific antibody (Ab)<sup>1</sup>. The large binding constant is exploited in Enzyme-Linked ImmunoSorbent Assay (ELISA) to detect the presence of biomarkers in bodily fluids whose concentration can be below picomolar level<sup>2</sup>.

Detecting Ab-Ag interactions with a label-free sensing scheme requires the integration of bio-recognition moieties at a solid-liquid interface and their coupling with the transducer. The transduction of the molecular binding event should occur with minimum, if not any, further chemical amplification or development steps<sup>3</sup>. This is particularly relevant for point-of-care applications and in-field deployed sensors. Sensitivity and specificity both depend on how the bio-recognition groups are made available to the target and on the coupling between environment and transducer.

Among label-free immunosensors, mechanical and electronic transductions have been demonstrated<sup>4-8</sup>. In the case of an electronic sensor, several phenomena induced by the bio-recognition event might be exploited: local changes of electrostatic potential<sup>9</sup>, density of charge carriers, conductivity<sup>10</sup>, impedance<sup>11</sup>, capacitance<sup>12</sup>. Simplicity of instruments and low cost are factors that make electronic transduction favoured for single-shot applications<sup>13</sup>. Device sensitivity is optimized by tuning the Debye length scale in biological fluids to the size of the specific binding pair. However the modulation of the Debye length is not always doable<sup>14-16</sup>, especially in bodily fluids.

Mechanical sensors, such as quartz crystal microbalance (QCM)<sup>5</sup> and cantilevers<sup>6</sup>, detect changes of mass, binding/unbinding forces and viscoelastic response. They are effective in those

1  
2  
3 regimes where electronic sensing does not provide enough sensitivity. However the interpretation  
4 of the device output in terms of specific molecular interactions is not usually straightforward.  
5  
6  
7

8  
9 Quantification, reproducibility and standardization are open issues in label-free  
10 immunosensing. They require multi-scale control from nanometer to hundreds of micrometers of  
11 the density, orientation and functionality of the recognition moieties on the sensing area of the  
12 device. Open questions, that also represent technological challenges, include: how to control the  
13 density of active Abs; what fraction of Abs gives rise to specific bio-recognition events; what is  
14 the detection limit of the device in terms of number of recognition events; how to make the  
15 device more effective, sensitive, and specific.  
16  
17  
18  
19  
20  
21  
22  
23  
24

25 In this Paper, we propose a multi-scale approach, combining local and non-local  
26 techniques that serve to quantify antibody-antigen recognition events in label-free electronic  
27 biosensors. Our approach combines an electrolyte-gated organic field effect transistor  
28 (EGOFET) (Fig.1) and single molecule force spectroscopy (SFS) (Fig. 2) to assess specific  
29 recognition on device-relevant Au surfaces in the limit of strong electrostatic screening regime.  
30  
31  
32  
33  
34  
35  
36

37 In EGOFET the gate electrode immersed in the electrolyte solution is functionalized with  
38 a bio-recognition moiety. In the presence of the target molecule in solution, a number of local  
39 binding events at the gate electrode leads to a potential change<sup>17-19</sup>. This change affects the  
40 electrostatic potential at the electrolyte solution/organic semiconductor interface, which  
41 couples to the semiconductor channel via the capacitance  $C_{DL}$  of the Debye-Helmholtz layer.  
42 Being  $C_{DL}$  on the order of 10-20  $\mu\text{F}/\text{cm}^2$ ,<sup>20</sup> EGOFET responds to changes of potential as low as  
43 50-100  $\mu\text{V}$ .<sup>21</sup> These correspond approximately to a few recognition events per 100x100  $\text{nm}^2$   
44 area of the device. Considering an active channel area  $A=W\cdot L$  given by width  $W$  multiplied by  
45 length  $L$ , EGOFET with  $A=1 \text{ mm}^2$  responds to 10-100 million recognition events occurring on  
46  
47  
48  
49  
50  
51  
52  
53  
54  
55  
56  
57  
58  
59  
60

1  
2  
3 the device. EGOFETs were shown to transduce signals in neuronal cell populations, sub-nM  
4 concentration of neurotransmitters<sup>22</sup> and DNA<sup>23</sup>, local pH changes (9mV/pH)<sup>24</sup>, penicillin<sup>25</sup>  
5 and biotin-streptavidin hybridization<sup>26</sup>.  
6  
7

8  
9  
10 SFS is instead sensitive to a few single antibody-antigen interactions. In SFS, the force  
11 dependence on the probe-surface distance, termed force curve, is recorded. A force curve  
12 exhibits regions where a smooth variation vs the distance is interrupted by abrupt changes.  
13 These “jumps” are interpreted as the rupture of single or multiple bonds that were formed  
14 because of molecular recognition interactions. The value of the forces measured by SFS  
15 depends on both the loading rate<sup>27,28</sup> and the relevant electrostatic interactions<sup>29</sup>. Being the  
16 latter anisotropic, the orientation of the recognition moiety on the surface is important. This  
17 orientation may substantially vary depending on the protocol adopted for immobilizing the  
18 recognition group on the surface. SFS has been successfully applied to measure the forces  
19 between ligands and receptors<sup>30,31</sup>, antibody-antigen<sup>32,33</sup>, to investigate the unfolding of  
20 proteins<sup>34</sup>, protein stability<sup>35</sup>, the interaction between carbohydrates<sup>36</sup>, and cell adhesion<sup>37</sup>.  
21  
22  
23  
24  
25  
26  
27  
28  
29  
30  
31  
32  
33  
34  
35

36 Here the analytical target is interleukin-4 (IL4), an anti-inflammatory cytokine relevant in  
37 several pathologies<sup>38-41</sup>. We adopt IL4 monoclonal antibody as the specific recognition moiety  
38 in EGOFET and SFS. Two distinct Ab-immobilization protocols on the gate electrode have  
39 been compared. The first is based on 6-aminohexanethiol (HSC6NH2) monolayer activated by  
40 glutaraldehyde<sup>42,43</sup>. This functional approach guarantees chemical binding between the metal  
41 and the side chains of the lysine residues in the Ab; however, it does not allow one to control  
42 the Ab orientation due to the natural abundance of lysine in the Ab backbone. The second  
43 strategy exploits the recombinant His-Tagged PG, whose N-terminus side is tailored by a 6-  
44 histidine chain (6-His-Tag). His-Tags are well-known to bind polycrystalline Au<sup>44,45</sup>. This  
45  
46  
47  
48  
49  
50  
51  
52  
53  
54  
55  
56  
57  
58  
59  
60

1  
2  
3 affinity was already exploited for the fabrication of nano-mechanical motors based on the  
4 grafting of F1-ATPase on gold substrates<sup>46</sup>. His-Tagged PG forms an oriented layer which  
5 promotes Ab immobilization on the Au electrode<sup>47</sup>. Neutron reflectometry, light interferometry  
6 and ellipsometry show that Abs on PG-functionalized ideal surfaces form smooth  
7 monolayers<sup>48</sup>. Antibodies are oriented by the specific interaction of PG with the fragment  
8 crystallizable region (Fc) that forces Ab to expose its binding sites to the environment<sup>49,50</sup>.  
9

10  
11 Our results show a substantial difference in EGOFET and SFS responses to IL-4 when its  
12 antibody is immobilized on 6-His-Tagged PG/Au electrodes. EGOFET detects changes of  
13 charge mobility and threshold voltage for IL-4 concentrations as low as 5 nM. No change is  
14 detected on electrodes functionalized with HSC6NH2. SFS experiments allow us to estimate a  
15 larger probability of specific recognition events ( $P_{sb} \approx 30\%$ ) occurring on PG-functionalized  
16 electrodes with respect to the control samples ( $P_{sb} < 10\%$ ). Specific binding events display a  
17 mean (un-)binding force  $\approx 99$  pN, and  $\approx 109$  pN for PG- and HSC6NH2-functionalized ones,  
18 respectively. The respective dissociation time constants are in the 50:1 ratio. This evidence  
19 demonstrates that Ab-Ag pairs with larger conformational stability are more likely formed on  
20 PG functionalized electrodes, as a result of higher orientational order of the Ab on PG-  
21 functionalized Au electrodes.  
22  
23  
24  
25  
26  
27  
28  
29  
30  
31  
32  
33  
34  
35  
36  
37  
38  
39  
40  
41  
42

43 These results show the direct correlation between SFS measurements at the single  
44 molecule level and the electronic response of the EGOFET that is caused by a change of  
45 electrostatic potential on  $\text{mm}^2$  channel. The evolution of this approach leads to a methodology  
46 for optimization and reproducibility of label-free biosensors.  
47  
48  
49  
50  
51  
52  
53  
54  
55  
56  
57  
58  
59  
60

## 2. RESULTS AND DISCUSSION

### 2.1 Electrochemical measurements

The result of the functionalization of Au electrodes was first assessed by cyclic voltammetry and impedance spectroscopy (see Fig. 3) by monitoring the changes in the faradaic response of the ferricyanide redox probe,  $[\text{Fe}(\text{CN})_6]^{3-/4-}$ . In the case of HSC6NH<sub>2</sub>-functionalized Au electrodes, cyclic voltammetry displays an increase of the peak-to-peak distance from 60 mV to >250 mV upon changing the pH of the solution from neutral to basic values (Fig. 3a). This indicates a dramatic slowing down of the electron transfer, not observed on bare Au, that is consistent with the presence of the amino-terminated SAM on the electrode surface<sup>51</sup>.

We monitored PG adsorption onto polycrystalline Au electrodes by means of impedance spectroscopy (Fig. 3b). The data fitted with Randles circuit (see Experimental Section 4.3) show that the capacitance ( $C_{DL}$ ) decreases from 11.3(±0.2) μF to 2.1(±0.1) μF and  $R_{CT}$  increases from 12.8(±0.2) Ω to 270(±3) Ω. This indicates that PG is adsorbed onto Au electrode. The orientation of the adsorbed PG is assessed by measuring the impedance changes upon incubation of the PG-functionalized electrode in a 400 mM imidazole solution for 30 min. We observe a capacitance increase to 2.7(±0.1) μF, along with a dramatic decrease of  $R_{CT}$  down to 63(±0.1) Ω. These changes evidence partial desorption of His-Tagged PG from the gold electrode, thus proving that His-Tag mediates the PG assembly on Au (see Fig. 3b).

Both strategies are effective for immobilizing of anti-IL4 on the surface as apparent from Fig. 4 and the data reported in Table S1. For both electrode functionalizations, we observe a significant increase of the charge transfer resistance  $R_{CT}$  upon incubation in anti-IL4 solution. The capacitance change is consistent with the Ab adsorption for the HSC6NH<sub>2</sub>-functionalized

1  
2  
3 electrode. The capacitance exhibits no significant change in the case of PG-functionalized  
4  
5  
6 electrode.  
7

## 8 9 **2.2 Tapping mode AFM**

10  
11  
12 The ability of both functionalization protocols to lead to Ab immobilization onto the gold  
13  
14 substrate has been evaluated by tapping mode AFM in air and PBS medium. The surface  
15  
16 topography of a typical bare gold sample recorded in air is displayed in Fig. 5a. The sample  
17  
18 consists of few tens nm-diameter gold grains formed by thermal sublimation, with a maximum  
19  
20 height of 10 nm and root mean square (RMS) roughness of 1.1 nm. PG adsorption (Fig. 5b)  
21  
22 yields a smoother surface of reduced height and roughness. Incubation of the sample with the  
23  
24 anti-IL4 solution leads to an increase of the maximum height by 3.5 nm and roughness by 0.39  
25  
26 nm (Fig. 5c). The height difference is in good agreement with the size of IgG antibodies  
27  
28 adsorbed with an orientation consistent with the so-called Y configuration previously reported in  
29  
30 air<sup>52</sup>.  
31  
32  
33  
34

35  
36 The RMS roughness for the different functionalization steps (Fig. 5d) follows the same trend  
37  
38 both in air and in phosphate buffer solution (PBS). There is a decrease upon PG deposition that is  
39  
40 followed by an increase of 0.39 nm in air and 0.61 nm in PBS as a result of the antibody  
41  
42 immobilization.  
43  
44

## 45 46 47 **2.3 Single force spectroscopy**

48  
49  
50 After assessing the successful immobilization of anti-IL4 on modified gold substrates, bio-  
51  
52 molecular recognition has been studied by means of SFS using probes functionalized with IL-4  
53  
54 linked to the tip by a flexible PEGylated chain (see Experimental Section 4.4). The binding  
55  
56  
57  
58  
59  
60

1  
2  
3 forces between the specific probe and anti-IL4 bound to the electrode surface were extracted  
4  
5 from series of repeated force curves acquired on a 32 x 32 points grid on an area of 1  $\mu\text{m}$  x 1  $\mu\text{m}$   
6  
7 (see Experimental Section 4.4).  
8  
9

10 Fig. 6a and Fig. 6b show the 2D-histograms containing the number of events with a given  
11  
12 unbinding force ( $F_{ub}$ ) and unbinding length ( $L_{ub}$ ) for PG- and HSC6NH2-functionalized  
13  
14 electrodes, respectively. These histograms cluster together the curves with similar values of the  
15  
16 unbinding forces and unbinding distance. Each point (represented as an hexagon) in the 2D  
17  
18 histograms contains the force curves corresponding to different types of events. As an example,  
19  
20 Fig.s 6c and 6d show a representative force curve for one of the hexagons in Fig.s 6a and 6b. The  
21  
22 noisy and adhesive behavior observed in the force curves is related to the fact that the  
23  
24 measurements were performed on a real technological surface like polycrystalline gold, instead  
25  
26 of prototypical substrates such as mica, which is atomically flat on large areas and more  
27  
28 homogenous.  
29  
30  
31  
32

33 Regarding unbinding lengths, all events occur in the 20-40 nm range with a dispersion ranging  
34  
35 from 10 to >50 nm corresponding to the PG-coated Au surface. The most probable unbinding  
36  
37 lengths occur in the 10-20 nm range with dispersion ranging from 10 to 35 nm for anti-  
38  
39 IL4/HSC6NH2/Au surface. We infer that for PG/Au electrodes unbinding events are more spread  
40  
41 out at different lengths, and their unbinding distance is further away from the surface. This  
42  
43 observation is consistent with the presence of a larger fraction of oriented antibodies in a  
44  
45 standing Y-shape configuration<sup>53</sup>, since in this case we expect that the unbinding event take place  
46  
47 further away from the surface. Additionally, the Fab fragments of an IgG antibody are linked to  
48  
49 the Fc fragment through di-sulphide bonds, resulting in an increased flexibility of these  
50  
51 fragments<sup>54</sup>. Thus, an antibody in Y-shape configuration is less constrained by the substrate,<sup>5</sup> which  
52  
53  
54  
55  
56  
57  
58  
59  
60

1  
2  
3 explains the broader distribution of unbinding events in distance in the case of highly-oriented  
4 anti-IL4. For HSC6NH2 functionalization, our results suggest that the anti-IL4 is randomly  
5 oriented.  
6  
7  
8  
9

10  
11 We then performed a statistical analysis of the large dataset of (un-)binding forces  $F_{ub}$ . As  
12 shown in Fig.6e, both anti-IL4/PG/Au and anti-IL4/HSC6NH2/Au, along with the crosscheck  
13 sample (namely, tip functionalized with IL6 and Au electrode coated with anti-IL4) yield  
14 apparently skewed histograms of  $F_{ub}$ . This is not surprising because the data sets have been  
15 filtered out the aspecific events occurring at  $F_{ub} \leq 20$ pN. The size of the bin of each histogram is  
16 calculated depending on the number of curves  $N_{SB}$  in the data set giving rise to (high-force)  
17 specific (un-)binding ( $SB$ ). This number changes from sample to sample and therefore the sizes  
18 of histograms in Fig. 6 are different. Specifically, the number of bins in each histogram is chosen  
19 as  $N_{bin} = \text{NINT}(3.49 \cdot \sigma / N_{SB}^{1/3})$ , with NINT being the nearest integer round-off, and  $\sigma$  the standard  
20 deviation of the data set. The bin size of each histogram is given by  $\Delta F = (F_{max} - F_{min}) / N_{bin}$ , where  
21  $F_{max}$ ,  $F_{min}$  are the boundary values of the force range measured experimentally. The value of the  
22 histogram is normalized to the Specific Unbinding Probability Density (SUPD):  
23  
24  
25  
26  
27  
28  
29  
30  
31  
32  
33  
34  
35  
36  
37  
38  
39  
40

$$(1) \text{ SUPD}(F_k) \approx 100 \frac{N_{SB}}{N_{TOT}} \left[ \frac{1}{\Delta F} \frac{N_k}{N_{SB}} \right]$$

41  
42 where  $N_k$  is the number of curves in the  $k$ -th bin whose unbinding force  $F_{ub}$  falls within  $F_k \pm \Delta F/2$ .  
43  
44  
45  
46 Its integral vs  $F_{ub}$  across the data set is estimated as the summation on the histogram bins  
47 multiplied by  $\Delta F$ . The summation index runs from 1 to  $k_{max}$ ,  $k_{max}$  being the index corresponding  
48 to  $F_{k_{max}}(F_{ub})$ . The Specific Unbinding Probability  $\text{SUP}(F_{max}) = 100 \cdot N_{SB} / N_{TOT}$  is the asymptotic  
49 limit of the curves shown in Fig. 6f:  
50  
51  
52  
53  
54  
55  
56  
57  
58  
59  
60

$$(2) \text{ SUP}(F_{ub}) = \int_0^{F_{ub}} \text{SUPD}(F) dF \approx 100 \left[ \sum_{k=1}^{k_{\max}} \frac{N_k}{N_{TOT}} \right]$$

The skewness (standardized third moment) of each data set is found to be significant as its values largely exceed the corresponding Gaussian distribution estimator  $\sqrt{6/N_{SB}}$ <sup>55</sup>. The three data sets exhibit a mean force value  $\langle F_{ub}^* \rangle (\pm \sigma)$  equal to 98( $\pm 55$ ) pN, 109( $\pm 59$ ) pN and 80( $\pm 39$ ) pN for PG, HSC6NH2, and crosscheck samples respectively. We have inserted these values as parameters in the functional<sup>56,57</sup>,

$$(3) \text{ SUPD}(F_{ub}) = 100 \cdot \frac{N_{SB}}{N_{tot}} \cdot \chi^2(F_{ub}) = 100 \cdot \frac{N_{SB}}{N_{tot}} \frac{1}{2^p \Gamma(p)} \left( \frac{\sqrt{p} \cdot F_{ub}}{\sigma} \right)^{p-1} \exp\left( -\frac{\sqrt{p} \cdot F_{ub}}{\sigma} \right)$$

Eq. 3 describes a chi-square distribution normalized to the overall probability to detect a specific

(un-)binding event. Here the parameters are:  $p = \left( \frac{\langle F_{ub}^* \rangle}{\sigma} \right)^2$ ,  $\Gamma(p)$  is the gamma function. The

trends of SUPD, depicted as continuous curves overlapping the histograms in Fig. 6e, show a conformational adherence within the force range from 20 pN to 300 pN<sup>58-62</sup>. It is clear that the SUPD curves for both PG and HSC6NH2 are alike, and can be mapped one onto another by a simple vertical rescaling. On the other hand, they are substantially different from the one of crosscheck sample that has the same shape but whose peak is displaced at lower force values, and they are radically different from the one of the control sample (bare Au) that does not exhibit an apparent skewness. By looking at the SUP it is clear that anti-IL4/PG/Au induces a three-times larger frequency of specific binding events than the sample anti-IL4/HSC6NH2/Au (see Fig.6f). These values can be interpreted as the result of the effective coverage of functional Abs on the respective surfaces, viz. PG yields a 30% coverage of available Abs for recognition of

1  
2  
3 IL4, whereas HSC6NH2 only 10%. The comparison between the two immobilization strategies  
4  
5 has been reproduced with another antibody-antigen pair, viz. interleukin-6 (IL-6)/anti-IL6 pair,  
6  
7 yielding even more marked differences in recognition probability (see Fig.S5 Supporting  
8  
9 Information). Noticeably, the SUP of HSC6NH2 is comparable to that of crosscheck sample,  
10  
11 although it appears that the latter is contributed to events whose force is below 200 pN. This  
12  
13 implies that in the crosscheck sample it is possible to observe single specific recognition events,  
14  
15 but not multiple ones, conversely to the other cases. The distribution related to bare gold shows a  
16  
17 different trend, and the SUP is much lower than all the other distributions. This means that IL4  
18  
19 poorly interact with un-functionalized Au, as expected.  
20  
21  
22  
23  
24

25  
26 In order to gain insights into the energy landscape of the bound complexes, we carried  
27  
28 out experiments at different retraction velocities. According to the Bell-Evans model, the force of  
29  
30 a single-energy barrier in the thermally activated regime scales up with the logarithm of the  
31  
32 loading rate<sup>28</sup> (see Supporting Information 4.4):  
33  
34

$$(4) \quad F_{ub} = \frac{k_B T}{x_\beta} \ln \left( \frac{\nu x_\beta}{k_{off} k_B T} \right)$$

35  
36 Here  $F_{ub}$  is the most probable unbinding force,  $\nu$  the loading rate,  $x_\beta$  the position of the energy  
37  
38 barrier along the reaction coordinate,  $k_{off}$  is the dissociation constant at zero force and  $k_B T$  is the  
39  
40 thermal energy.  
41  
42

43  
44 The associated values for the Bell-Evans model parameters such as the reaction length  $x_\beta$  and the  
45  
46 lifetime of the complex  $\tau=1/k_{off}$  are reported in Table II. The value of the  $k_{off}=4*10^{-3} \text{ s}^{-1}$ ,  
47  
48 corresponding to  $\tau=206 \text{ s}$  for PG-based functionalization, is in good agreement with the values  
49  
50 observed in literature for specific antigen-antibody pairing characterized by single molecule  
51  
52 force spectroscopy<sup>58,63</sup>. For HSC6NH2-functionalization, we obtain  $k_{off}=0.209 \text{ s}^{-1}$ , corresponding  
53  
54  
55  
56  
57  
58  
59  
60

1  
2  
3 to a lifetime  $\tau=4.78$ s. The almost two orders of magnitude ratio of the  $k_{off}$  indicates that the  
4 antigen fits more steadily the antibody when the latter is immobilized onto the PG substrate, as  
5 compared to the HSC6NH2-functionalization<sup>64,65</sup>. This yields the increased binding affinity  
6 between IL4/anti-IL4 when PG is used for the antibody immobilization. As far as the potential  
7 barrier width between the bound complex and the transition state,  $x_{\beta}$ , is concerned, the values for  
8 both functionalization approaches fall in the range usually found for specific interactions  
9 between partners with a rather high conformational stability<sup>53</sup>. We observe that the IL4/anti-IL4  
10 complex formed via PG immobilization with a lifetime of the complex of 206s shows higher  
11 stability as compared to the one formed onto the SAM-functionalized surface, which will  
12 dissociate faster at a complex lifetime of 4.78s.  
13  
14  
15  
16  
17  
18  
19  
20  
21  
22  
23  
24  
25  
26

27 According to the Evans Bell model, the dissociation of the antibody-antigen complex under an  
28 external force is described in the frame of the transition state theory<sup>27,66</sup>. One  $k_{off}$  is calculated,  
29  $\Delta G$  can be estimated using the following equation, where  $h$  is Planck's constant:  
30  
31  
32  
33  
34

$$(5) \quad \Delta G = -k_B T \ln \frac{k_{off} \cdot h}{k_B T}$$

35  
36  
37  
38  
39  
40 The total free energy of the antibody-antigen complex has been estimated for the two gold  
41 functionalization approaches, obtaining values of -91 kJ/mol for the PG mediated  
42 functionalization and -82 kJ/mol for the HSC6NH2-functionalization. One should take into  
43 account the fact that this free energy includes contribution from the unbinding process of the  
44 antibody-antigen complex, as well as from the stretching of the PEG linker. Therefore, the free  
45 energy related exclusively to the unbinding process of the IL4/anti-IL4 complex can be  
46 calculated from this expression:  
47  
48  
49  
50  
51  
52  
53  
54  
55  
56  
57  
58  
59  
60

$$(6) \quad \Delta G_{ub} = \Delta G_{Ab/Ag} - \Delta G_{PEG}$$

The free energy related to the stretching of a 10 nm long PEG linker has been estimated experimentally to be  $-7.45 \text{ kJ/mol}^{67}$ , so the unbinding free energy corresponding to the antibody-antigen pairs are  $-84(\pm 42) \text{ kJ/mol}$  for the PG-based functionalization and  $-75(\pm 26) \text{ kJ/mol}$  for the HSC6NH2 functionalization. These values of the unbinding free energy could be related to the breaking of several hydrogen bonds and one or two salt bridges that are responsible of the Ab-Ag recognition.

#### 2.4 Detection of IL4 with EGOFET-based immunosensors

The pristine device exhibits a field-effect charge mobility  $\mu = 3.8 \times 10^{-4} \text{ cm}^2 \text{V}^{-1} \text{s}^{-1}$  and a threshold voltage  $V_{th} = -40 \text{ mV}$ . The leakage current is always lower than  $10 \text{ nA}$  along with an almost negligible hysteresis featuring no electrochemical doping of pentacene thin-film.

The I-V characteristics of an immuno-EGOFET with a gate electrode modified with anti-IL4, immobilized by glutaraldehyde-based protocol, is shown in Fig. 7a. We observe that the anti-IL4 (red curve) induces an electrical change in the I-V curve with respect to that recorded before anti-IL-4 immobilization (black curve). The Au gate electrode was then incubated in a reference solution of IL-4 at a concentration of  $5 \text{ nM}$ . This additional exposure does not give rise to further electrical change (blue curve). According to the protocol of Porter et al.<sup>68,69</sup>, the biological layer has been electrochemically detached (see Fig. S4 in supporting info) via the cleavage of the chemical bond between Au and sulphur of the 6-aminohexanethiol. The subsequent increase of the EGOFET performance proves that no deterioration is taking place at the experimental time-scale. The same validation process has been applied to the PG-based protocol (see Fig. 3b). At

1  
2  
3 variance with the previously described case, a significant change in the electrical response is now  
4  
5 observed after incubation of the gate electrode in the IL-4 solution.  
6  
7

8  
9 We then focused our attention only on the PG-mediated functionalization and monitored step-by-  
10  
11 step changes in the electrical performances of the device by recording shifts of  $\mu$  and  $V_{th}$  (see  
12  
13 Fig. 7c and Fig. 7d). Throughout the functionalization procedure, mobility shows a gradual  
14  
15 decrease down to 60% of the initial value. This is ascribed to a decrease of the capacitive  
16  
17 coupling between the gate electrode and the organic semiconductor thin film due to addition of  
18  
19 biological layers on the gate surface (see Fig. 7c). Regarding the threshold voltage, a rather  
20  
21 complex behavior has been observed. On one hand, the adsorption of protein G gives rise to a  
22  
23 negative shift of threshold voltage, while on the other hand both anti-IL4 grafting and  
24  
25 subsequently IL-4 recognition yield an opposite shift. This means that the protein G reduces the  
26  
27 charge-carrier density in the conductive channel with respect to bare Au electrode. Owing to the  
28  
29 fact that the isoelectric point (pI) of protein G is acidic (around 5), this means that protein G is  
30  
31 negatively charged at pH=7.2 and strongly coupled to the charge carriers in the channel to act as  
32  
33 a trap, and not as a dopant. In the case of IL-4 whose pI=8.2, there is a partial release of these  
34  
35 “trapped” carriers manifesting itself with a shift towards less negative threshold voltage. This can  
36  
37 be due either to formation of a surface dipole upon specific binding of IL-4 to its anti-IL4, thus  
38  
39 increasing the capacitance of the interface and the consequent capacitive coupling, or to a partial  
40  
41 compensation of the negative charge density of protein G.  
42  
43  
44  
45  
46  
47  
48  
49

50 Our electrical measurements show that PG functionalized EGOFETs are capable to sense IL4  
51  
52 down to 5 nM concentrations, while the HSC6NH2 functionalized device does not give a  
53  
54 measurable response. Protein G functionalized device shows a mobility loss of 16% and a  
55  
56 positive shift in the threshold voltage of approximately 10 mV after exposure to an IL-4 solution  
57  
58  
59  
60

1  
2  
3 (see Table I). The absence of significant changes in the electrical properties EGOFETs with gate  
4  
5 electrodes modified with the HSC6NH<sub>2</sub>-based functionalization is consistent with the much  
6  
7 lower probability of recognition events for randomly oriented anti-IL4.  
8  
9

### 10 11 3. CONCLUSIONS 12 13

14  
15 The detection of the bio-molecular recognition between interleukin-4 and its specific  
16  
17 antibody by electrolyte-gated organic field-effect transistor and force spectroscopy  
18  
19 measurements involves different processes, spatial and temporal scales. While EGOFET  
20  
21 detection involves change of electrostatic charge due to about  $10^{12}$  local recognition events per  
22  
23  $\text{cm}^2$ , SFS involves the detection of a few biorecognition events occurring at nm length-scales.  
24  
25 For this reason, comparing and complementing the results acquired with the two techniques is a  
26  
27 challenging task whose correlation is not trivial. We have successfully merged the evidences  
28  
29 obtained by electrical and mechanical techniques to comparatively assess two immobilization  
30  
31 protocols for anti-IL4 on polycrystalline Au. The success of EGOFET in detecting nanomolar  
32  
33 concentrations of IL4 in the case of protein G mediated Ab immobilization correlates with the  
34  
35 larger areal density of available anti-IL4 antibodies as evidenced by SFS measurements,  
36  
37 corresponding to 30% coverage with respect to just 10% in the case glutaraldehyde-based  
38  
39 immobilization. While there is no substantial difference in the distribution of the specific binding  
40  
41 force for the two immobilization schemes, there is a marked difference in the kinetic constants,  
42  
43 that show a longer average lifetime of the antibody-antigen complex,  $\tau = 206(\pm 103)$  s, and a  
44  
45 closer bond,  $x_\beta = 3.2(\pm 0.2)$  nm, for the anti-IL4/Pg/Au. This shows that the local environment of  
46  
47 the available antibodies, which is subtly affected by the density and orientation of other  
48  
49 antibodies, is important in determining the effectiveness of the local recognition event. Our  
50  
51 comparative study demonstrates that the optimum antibody functionality towards its antigen is  
52  
53  
54  
55  
56  
57  
58  
59  
60

1  
2  
3 achieved for the PG-mediated anchoring and that achieving this high density of available  
4 antibodies is crucial for enhancing the label-free detection of the relevant protein.  
5  
6  
7  
8  
9

## 10 **4. EXPERIMENTAL METHODS**

### 11 **4.1. Device fabrication**

12  
13  
14  
15  
16 Our devices are prepared onto gold-coated glass slides purchased from Phasis (Switzerland).  
17  
18 These substrates are made of quartz glass (1mm thick) and a gold layer of 50nm plus few nm of  
19 titanium as adhesive layer. Each test-pattern bears 4 transistors, whose channel length is 15 $\mu$ m  
20 and channel width equal to 27000  $\mu$ m. The fabrication is carried out by laser ablation with a  
21 short-pulsed Nd:YAG infrared (IR)-laser supplied by a laser scan marker (Scriba Nanotecnologie  
22 S.r.l., Bologna, Italy). The IR-Laser pulse frequency and intensity are optimized in order to find  
23 the best compromise between removal of the Au layer and roughening of the underlying quartz.  
24  
25 Typical operation is performed at a laser power of 8300W and a pulse of 10ns and a frequency of  
26 15500Hz. The laser focus is moved over the surface at a scan-rate of 2000 $\mu$ m/s. Details are  
27 described elsewhere<sup>70</sup>.  
28  
29  
30  
31  
32  
33  
34  
35  
36  
37  
38  
39  
40  
41

### 42 **4.2. Gate functionalization**

43  
44  
45 6-aminohexanethiol (HSC6NH<sub>2</sub>) and glutaraldehyde are purchased from Sigma-Aldrich and  
46 used without further purification. Recombinant PG, monoclonal anti-murine IL-4 (Anti-IL4), and  
47 recombinant murine IL-4 were purchased from Vinci-Biochem S.r.l. (Firenze, Italy). These  
48 biological species are produced by Biovision (San Francisco, USA). His-Tagged recombinant  
49 protein G lacks the albumin and cell membrane binding domains.  
50  
51  
52  
53  
54  
55  
56  
57  
58  
59  
60

1  
2  
3 The gate electrode is a polycrystalline Au wire (diameter equal to 1mm). First, this electrode  
4  
5 undergoes a standard cleaning procedure<sup>71</sup>: (i) immersion in a concentrated H<sub>2</sub>SO<sub>4</sub> at 100°C for  
6  
7 1h; (ii) 20 cycles of electro-polishing by sweeping the potential from 0V to 1.5V in H<sub>2</sub>SO<sub>4</sub> (1M).  
8  
9  
10 The glutaraldehyde-based functionalization occurs by immersing the gate electrode in a 6-  
11  
12 aminohexanethiol solution (1mM) overnight. The further activation is achieved by using  
13  
14 glutaraldehyde solution (2.5%v/v) for 1h at 5°C and then the functionalized electrode is  
15  
16 immersed in an antibody solution (0.25mg/ml anti-IL4) for 1h at 5°C. The last step consists of  
17  
18 immersing the Ab-coated electrodes in buffer solution (100mM of PBS, pH 7.4) IL-4 (5nM). The  
19  
20 other functionalization exploits a buffer solution (100mM of PBS pH 7.4) of protein G (5mg/ml).  
21  
22  
23  
24  
25 Ab and Ag solutions are the same of the previous protocol.  
26

### 27 28 **4.3. Electrical measurements**

29  
30  
31 All the electrochemical, morphological and mechanical investigations described so far proved  
32  
33 the possibility of successfully immobilizing anti-IL4 antibodies on functionalized gold surfaces.  
34  
35 SFS experiments have also suggested that the use of PG-based immobilization protocol  
36  
37 significantly enhances the probability of recognition events between the surface coated with anti-  
38  
39 IL4 and IL4. We then applied these immobilization strategies to the functionalization of the gate  
40  
41 Au electrode of EGOFETs to obtain an immunosensor. Our aim is to establish the minimum  
42  
43 detection level of IL4 in test solutions, and assess whether these concentration ranges are  
44  
45 comparable with biologically-relevant ones. We compared the electrical responses of EGOFETs  
46  
47 with gate electrodes functionalized with the different protocols to assess whether controlling the  
48  
49 orientation of the Abs on the surface would enhance the sensing capability of the  
50  
51 immunosensors.  
52  
53  
54  
55  
56  
57  
58  
59  
60

1  
2  
3 All the electrical measurements were performed with home-built EGFETs. As mentioned in  
4 the experimental methods (4.1), the electronic transducer was fabricated by means of laser  
5 ablation<sup>70</sup>. Particular attention has been paid to maximize the  $W/L$  ratio, which is the geometrical  
6 parameter scaling the drain-source current ( $I_{DS}$ ). This home-built EGFET has been operated in  
7 a buffer solution (100mM of PBS at pH 7) mimicking the physiological conditions. The buffer  
8 solution has been confined on top of the electronic transducer by means of a PDMS pool, as  
9 shown in the cross-section of Fig.1.

10  
11  
12  
13  
14  
15  
16  
17  
18  
19  
20  
21 Source, drain and gate electrodes were connected to a Keithley 2612 Source Meter. The  
22 electrical response was acquired by means of a probe station. All the electrical measurements  
23 were carried out in ambient atmosphere. The I-V transfer characteristics were performed by  
24 sweeping the gate-source voltage ( $V_{GS}$ ) from +0.2 V to -0.5 V while leaving the drain-source  
25 voltage constant at -0.5V (saturation regime) for the reference device. The I-V output  
26 characteristics were carried out by sweeping drain-source voltage ( $V_{DS}$ ) from 0 V to -0.5 V and  
27  $V_{GS}$  from 0 V to -0.5 V with step of 0.1 V. The  $V_{GS}$  scan rate is 20mV/s and 80mV/s for transfer  
28 and output characteristics respectively.

29  
30  
31  
32  
33  
34  
35  
36  
37  
38  
39  
40  
41 Electrochemical measurements are performed by an usual three-electrodes cell connected to a  
42 potentiostat/galvanostat  $\mu$ -Autolab type III (Metrohm Italiana S.r.l., Varese, Italy), using a  
43 polycrystalline Au wire, as working electrode, functionalized with the above-mentioned  
44 protocols; a Pt sheet and Ag/AgCl were used as counter and reference electrodes respectively.

45  
46  
47  
48  
49  
50  
51 The impedance response is fitted by Randles circuit, which is an equivalent circuit composed by  
52 an electrolyte solution resistance,  $R_S$ , a charge transfer resistance,  $R_{CT}$ , a Debye-Helmhotz  
53 capacitance,  $C_{dl}$  and a Warburg element,  $W$ .

#### 4.4. Single molecule force spectroscopy measurements

In these experiments, the force dependence on the probe-surface distance is recorded (viz. force curve). A force curve contains regions that show a smooth variation with the distance. Those regions are interrupted by the presence of sharp changes in the force, which are associated with molecular recognition interactions, interpreted as the rupture of one or several bonds. The forces measured by force spectroscopy are dynamic in nature, as they depend on the loading rate<sup>27,28</sup> and electrostatic interactions<sup>29</sup>. To certain extent, the electrostatic interactions are controlled by the immobilization protocols applied to a bio-specie of interests on a certain substrate.

##### 4.4.1. Tip functionalization

Phosphate buffer saline powder which yields 0.01 M phosphate buffered saline (NaCl 0.138 M; KCl 0.0027 M) when dissolved in 1 liter of water, hydrogen peroxide 30%, sulphuric acid, 3-aminopropyl-triethoxysilane (APTES), glutaraldehyde 8%, 6-aminohexanethiol and ethanol were purchased from Sigma Aldrich. The 24-unit ethyleneglycol functionalized with succinimidyl and maleimido ends (NHS-PEG<sub>24</sub>-Mal) and the sulfhydryl addition kit containing: SATA (*N*-succinimidyl-S-acetylthioacetate), hydroxylamine•HCl, conjugation buffer stock (10X), dimethylformamide and Dextran desalting column were purchased from Thermo Scientific. Recombinant protein G, monoclonal anti-murine IL-4 and recombinant murine IL-4 are produced by Biovision (San Francisco, USA).

AFM silicon nitride tips were first cleaned thoroughly by immersion in a piranha solution (3:1 concentrated sulfuric acid to 30% hydrogen peroxide solution) for 30 minutes. They were then rinsed with nanopure water and dipped into a solution of 3-aminopropyl-

1  
2  
3 triethoxysilane:water:ethanol (ratio 5:5:95 v/v ) for 30 minutes. Finally, the amino-functionalized  
4  
5 tips were rinsed with nanopure water, ethanol and nitrogen dried.  
6  
7

8  
9 Next, the heterobifunctional NHS-PEG<sub>24</sub>-Mal linker was reacted with the antigen bearing a  
10  
11 sulfhydryl group. Prior to that, free sulfhydryl functionality was added to the antigen using the  
12  
13 SATA reagent. A 17.3 mM SATA solution in DMF was added in 10-fold molar excess to 1 mL of  
14  
15 protein. The reaction was incubated for 30 minutes at room temperature. Then, 5 mg  
16  
17 Hydroxylamine·HCl was mixed with 100 µl Conjugation Buffer Stock (10X). To de-protect the  
18  
19 latent sulfhydryl, 100 µl of hydroxylamine solution was added to the SATA-modified protein and  
20  
21 the mixture was incubated for 2 hours at room temperature. The de-protected sulfhydryl protein  
22  
23 was then added to the equilibrated desalting column to remove non-reacted reagents. The  
24  
25 maleimide conjugation buffer was added to the desalting column and 1 mL fractions were  
26  
27 collected and the absorbance of each fraction was measured at 280 nm to locate the protein.  
28  
29 Fractions containing most of the protein were then reacted with the NHS-PEG<sub>24</sub>-Mal linker. A  
30  
31 10-fold molar excess of the PEG linker was incubated with the sulfhydryl-modified antigen at  
32  
33 4°C for 12 hours. Finally, the amino-functionalized AFM tips were immersed in the PEG-antigen  
34  
35 solution for 2 hours at room temperature. The tips were when rinsed with PBS 0.1 M and stored  
36  
37 in a Petri dish at 4°C until further usage.  
38  
39  
40  
41  
42  
43  
44

#### 45 46 **4.4.2. Substrate functionalization**

47  
48 The substrates used were mica sheets covered with a 3 nm adhesive Cr layer and a 50 nm thick  
49  
50 gold layer. The antibody immobilization onto the gold substrate has been performed by  
51  
52 following the same protocols used for the gate functionalization (section 4.2).  
53  
54  
55

#### 56 57 **4.4.3. Topography measurements**

1  
2  
3 Tapping mode AFM was employed to record topographical images of the samples at different  
4 functionalization steps in both air and PBS<sup>72</sup>. Rectangular PPP-NCH (Nanoworld AG,  
5 Switzerland) cantilevers with a nominal force constant  $k= 40 \text{ N m}^{-1}$  and a resonant frequency of  
6 291 kHz have been used for air measurements. As for the experiments in liquid environment,  
7 rectangular OMCL-RC800PSA (Olympus, Japan) with a nominal force constant of 0.4 N/m and  
8 a resonant frequency of 33 kHz were employed. The topography measurements were performed  
9 in amplitude modulation AFM by driving mechanically the cantilever<sup>73</sup>.

#### 20 21 **4.4.4. Single molecule force spectroscopy measurements**

22  
23 Single molecule force spectroscopy experiments were performed with a Multimode atomic force  
24 microscope fitted with a Nanoscope V controller (Bruker, Santa Barbara). The microscope is  
25 equipped with a liquid cell where approximately 60  $\mu\text{l}$  of PBS 0.01M pH= 7.4 are introduced in  
26 order to carry out the measurements. Triangular silicon nitride tips OTR-4 (Bruker, Santa  
27 Barbara) with a spring constant of 0.015 – 0.08 N/m and resonant frequency of 1.8 kHz and 8  
28 kHz were used. The force constant and quality factor are determined by using the thermal noise  
29 method<sup>74</sup>. At the end of each experiment, the optical lever sensitivity was calibrated by  
30 acquiring deflection versus distance curves on a hard surface (mica). Typically 100 deflection vs  
31 distance curves are acquired and the sensitivity of the photodiode is calculated as the mean value.  
32 The force is calculated using Hooke's law:  $F = -kd$  ( $d$ = cantilever deflection,  $k$ =cantilever force  
33 constant). The applied force was maintained below 600 pN.  
34  
35  
36  
37  
38  
39  
40  
41  
42  
43  
44  
45  
46  
47  
48  
49  
50

51 The force curves were acquired in static mode by approaching and retracting the tip toward the  
52 sample by 200 nm at different velocities (0.5, 1, 2 and 5 Hz). Each time, the tip was kept in  
53 contact with the sample for 0.5 s in order to favor the recognition process.  
54  
55  
56  
57  
58  
59  
60

1  
2  
3 Several rounds of control experiments have been performed to check the specificity of the  
4 unbinding events. On one hand, force curves of a bare AFM tip interacting with the substrate at  
5 each functionalization step for both protocols were recorded. Afterwards, antigen tethering AFM  
6 tips were tested against Au, anti-IL4/HSC6NH2/Au and anti-IL4/Pg/Au. On the other hand,  
7 cross-reactivity experiments have been performed by bringing IL4 antibodies on the substrate in  
8 contact with the IL6 antigen on the tip.  
9

#### 10 11 12 13 14 15 16 17 18 **4.5 Dynamic force spectroscopy data analysis** 19

20  
21 A total of 16297 force distance curves were analyzed by using customized software in an  
22 automated way. The curves were averaged and the contact point was set according to a deflection  
23 threshold. Event recognition was based on the values of the second and third derivatives of the  
24 deflection; the event was labeled as a recognition event whenever the derivatives were found to  
25 be above a threshold with respect to the noise level. An algorithm was created to discriminate  
26 specific recognition events from surface adhesion events. The algorithm is based on the  
27 calculation of the deviation between the deflection curve and the straight line that goes from the  
28 peak minimum to the contact with the surface (see Supporting Information 4.5). Tables  
29 containing information on specific events for all the experiments were processed and 1D and 2D  
30 histograms were extracted. 1D histograms have been normalized to the number of force distance  
31 curves for every set of experiments. 2D histograms represent the number of specific events that  
32 occur which a given binding length and a given binding force. The binning sites for the binding  
33 length and force were set to 3 nm and 13 pN respectively.  
34  
35  
36  
37  
38  
39  
40  
41  
42  
43  
44  
45  
46  
47  
48  
49  
50  
51

52  
53 The dynamics of the IL4 antibody-antigen binding was explored by determining the unbinding  
54 force as a function of the unbinding rate. The loading rate is the product between the retract  
55  
56  
57  
58  
59  
60

1  
2  
3 velocity and the spring constant. To account for the contribution of the PEG linker spring  
4 constant to the overall spring constant of the system, the loading rate was extracted from the  
5 slope of the force curve before unbinding occurs. The plots in figure S5 display the linear  
6 increase of the most probable unbinding force with the logarithm of the loading rate for the two  
7 antibody immobilization protocols. This characteristic behavior for a thermally activated  
8 dissociation process under an applied load has been previously observed for other antibody-  
9 antigen complexes.

10 To determine the kinetic parameters of the molecular recognition process, the length of the  
11 energy barrier,  $x_{\beta}$ , was determined from the slope of linear fit of the unbinding forces vs. loading  
12 rate logarithm plot (see Eq.1). Next, the kinetic off-rate constant of dissociation at zero force was  
13 calculated by extrapolation to zero forces. Antibody-antigen complexes have limited lifetimes,  
14 which are shortened by thermal activation under an applied force. The characteristic time needed  
15 for the spontaneous dissociation,  $\tau$ , is given by the inverse of the kinetic off-rate constant and can  
16 be correlated with the specificity of the recognition process as well as the stability of the  
17 complex.

## 5. FIGURES

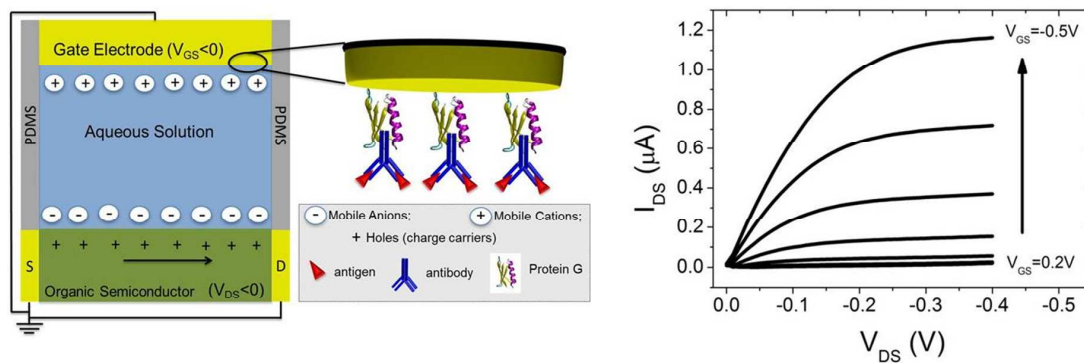


**Figure 1** On the left, a schematic EGO-FET cross-section along with a sketch of the magnification of the gate/electrolyte interface. On the right, I-V output characteristics of a reference device.

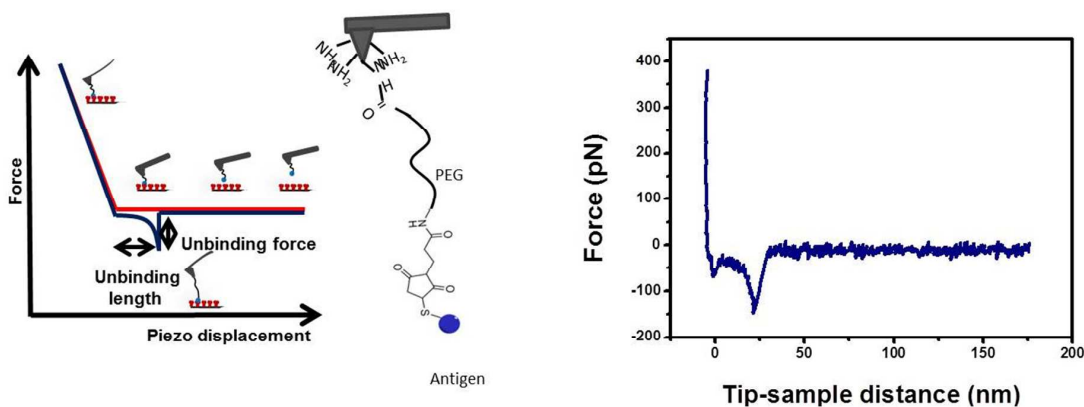


**Figure 2.** (Left) Schematics of a force-distance plot (force curve). As the tip approaches the sample, as contact is established the repulsive forces cause the tip to bend upwards (red line). The tip is then retracted (blue line). If a recognition event occurs, adhesion forces will make the tip to bend downward during retraction. When force gradient exceeds the spring constant of the cantilever, the probe jumps out of contact to its initial position. The unbinding force of the antibody-antigen pair is the maximum adhesive force, estimated as the vertical difference between the baseline and the minimum force at retraction. Unbinding length is the difference between the tip-sample distance where the unbinding event occurs and the contact point. Discrimination of specific and unspecific binding events relies on the estimate of the gradient of the force near the detachment point. Details are found in Supporting Information. (Center) Scheme of the AFM tip functionalization. IL-4- PEG linker complex is attached to an amino-functionalized AFM tip. (Right) Real force curve shows a specific unbinding event.

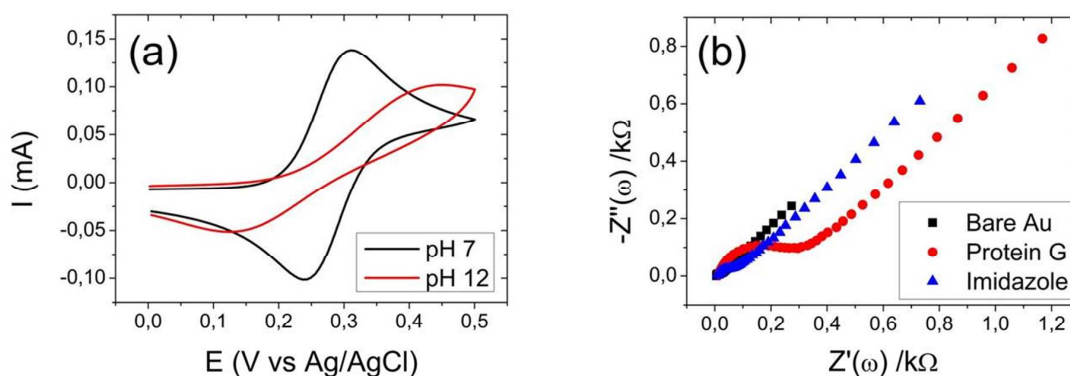


**Figure 3 (a)** Cyclic voltammograms of the ferricyanide signal at neutral and basic pH at a polycrystalline gold electrode functionalized with HSC6NH<sub>2</sub>. **(b)** Impedance spectroscopy for bare Au (black filled squares), PG adsorption (red filled circles) and PG elution mediated by imidazole exposure (blue filled triangles).

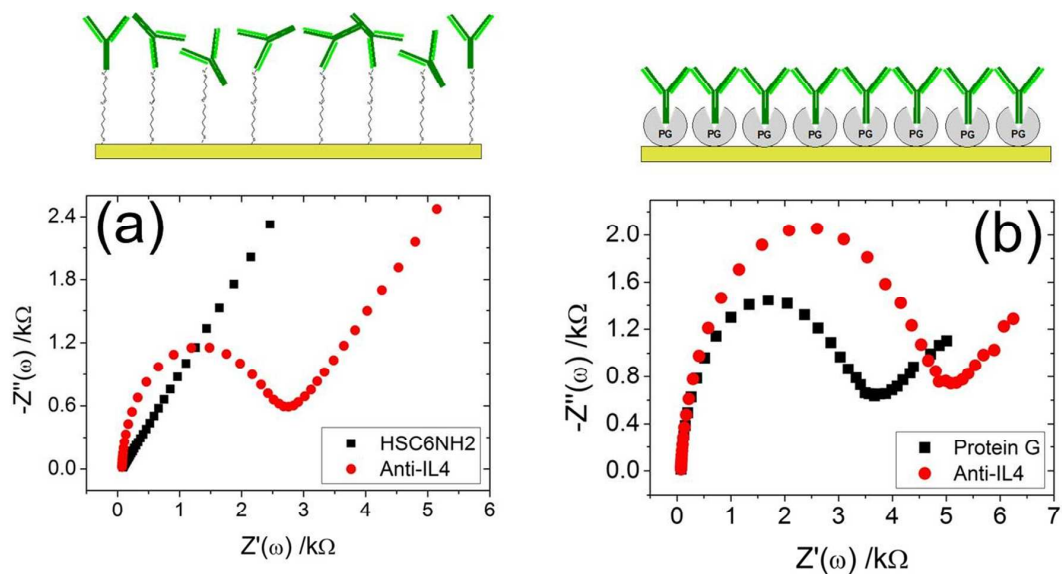


**Figure 4** Nyquist plots of (a) HSC6NH2- and (b) PG-mediated treatment. On the upper part of these plots, a cartoon of the two functionalization strategies is shown.

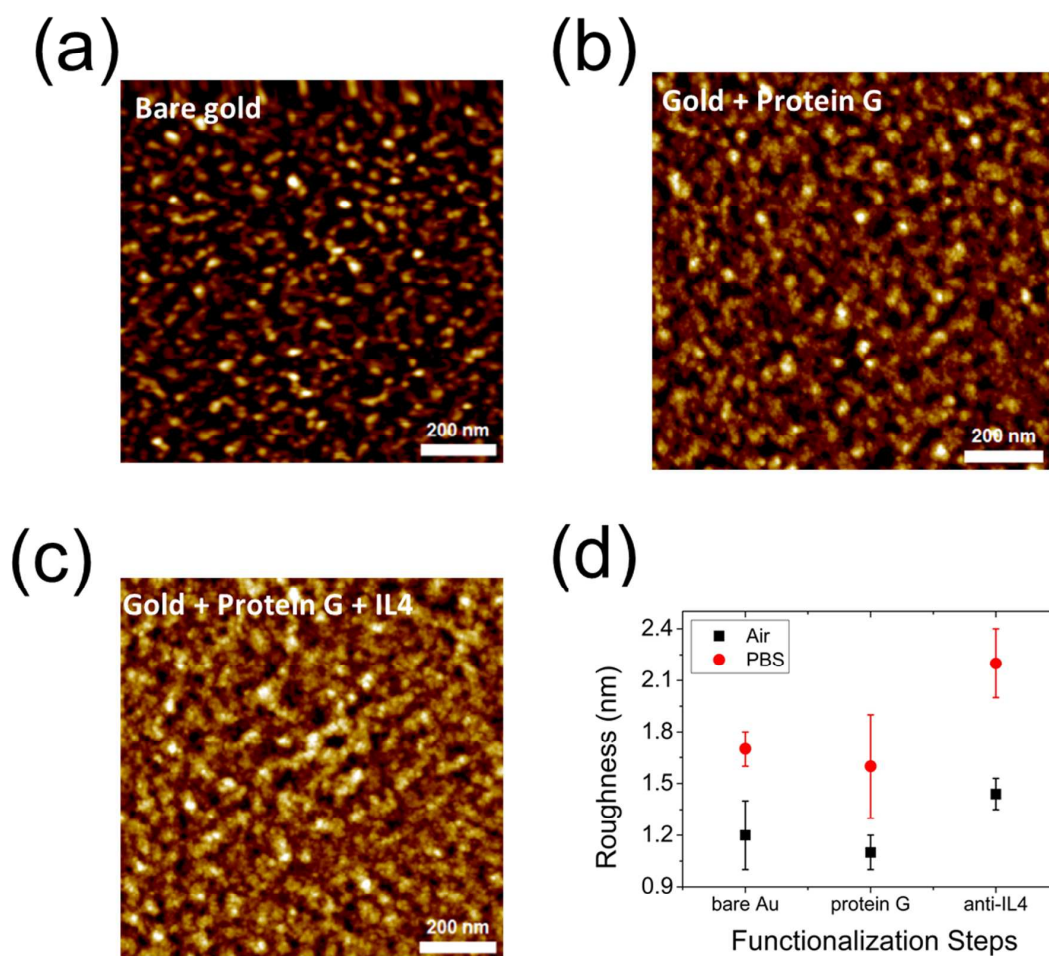


**Figure 5** AFM images on bare gold (a), PG-coated gold (b), PG/Anti-IL4-coated gold (c). Roughness data are overlaid in air and in PBS solution (d).

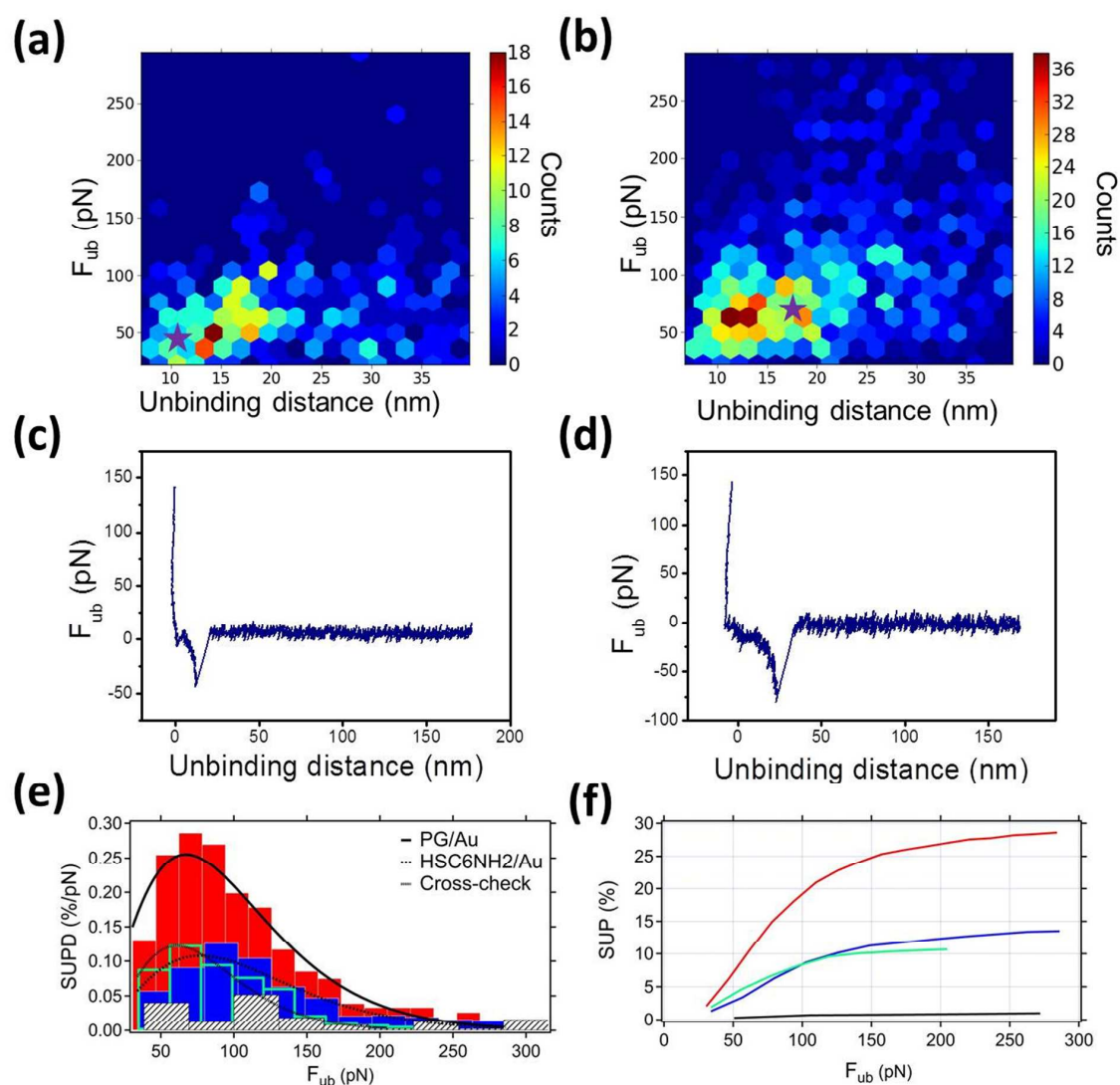


**Figure 6** 2D histograms of the unbinding distance and unbinding force for **(a)** GA-based protocol and **(b)** PG-based one. **(c-d)** Two representative Force vs distance curves corresponding to the starred hexagons in **(a)** and **(b)**. **(e)** Histograms of SPBD as a function of  $F$ . Red, blue, empty and white-black patterned bars stand for PG, GA, cross-check and bare Au respectively. Solid, dashed and dotted lines are the best  $\chi$ -square fits corresponding to PG, GA and cross-check **(f)** SUP vs.  $F$  plots are shown for each protocol.

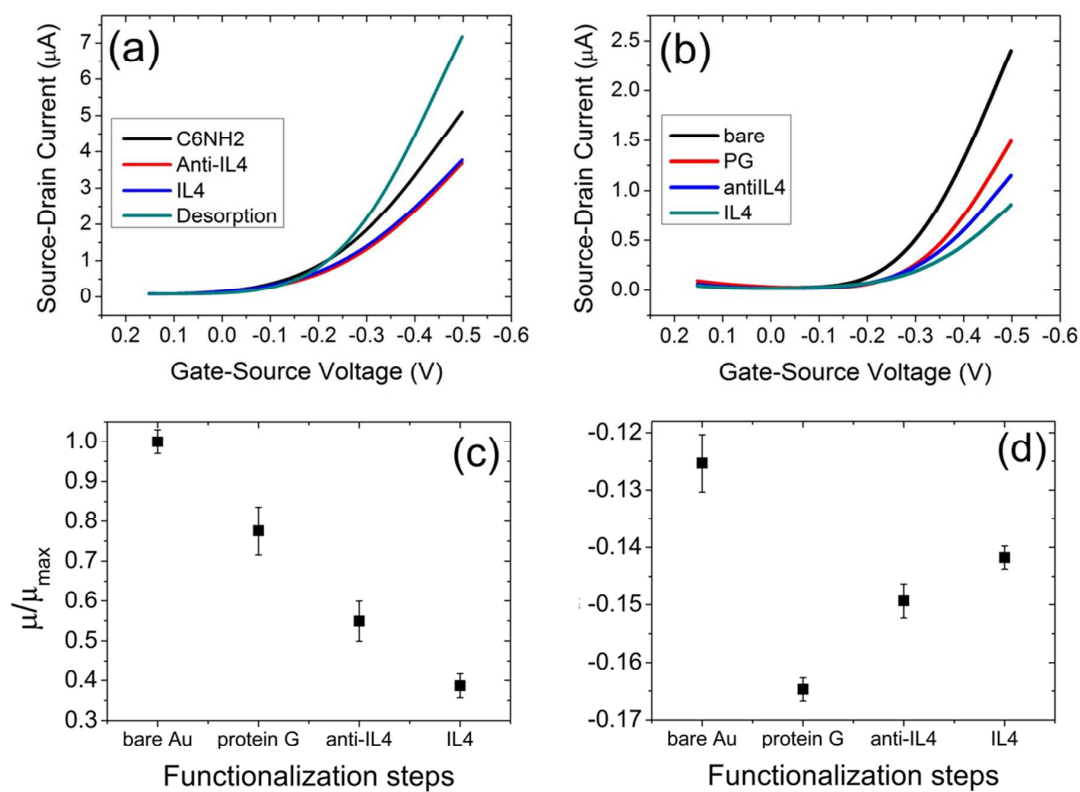


**Figure 7** I-V transfer characteristics for (a) HSC6NH2- and (b) PG-based protocols. Normalized mobility ratio (c) and threshold voltage (d) trends corresponding to the stepwise functionalization.

Table 1

Experiment	$x_{\beta}$ (Å)	$k_{\text{off}}$ ( $\text{s}^{-1}$ )	$\tau$ (s)	$\Delta G_{\text{binding}}$ (kJ/mol)	$\mu$ (% loss)	$\Delta V_{\text{th}}$ (mV)
<b>IL4 on Protein G</b>	3.2( $\pm$ 0.2)	0.004( $\pm$ 0.002)	206( $\pm$ 103)	84( $\pm$ 42)	16	$\approx$ 10
<b>IL4 on Glutaraldehyde</b>	2.4( $\pm$ 0.1)	0.209( $\pm$ 0.073)	5( $\pm$ 2)	75( $\pm$ 26)	-	-

## AUTHOR INFORMATION

## Corresponding Authors

\*Dr. Stefano Casalini, [stefano.casalini@unimore.it](mailto:stefano.casalini@unimore.it)

\*Prof. Ricardo Garcia, [r.garcia@csic.es](mailto:r.garcia@csic.es)

## Funding Sources

This work was supported by the EU-project I-ONE-FP7 “Implantable Organic Nano-Materials” NMP4-SL-2012, grant agreement n.280772.

## ACKNOWLEDGMENT

We thank Prof. Francesco Zerbetto, Alma Mater-Università di Bologna, for useful discussions.

## REFERENCES

- (1) Mariuzza, R. A.; Immunologie, D.; Pasteur, I.; Cedex, P. THE STRUCTURAL BASIS OF ANTIGEN-ANTIBODY RECOGNITION. *Annu. Rev. Biophys. Biophys. Chem.* **1987**, *16*, 139–159.
- (2) BK, V. W.; A.H.W.N., S. Immunoassay Using Antigen-Enzyme Conjugates. *FEBS Lett.* **1971**, *15*, 232–236.
- (3) Marquette, C. a; Blum, L. J. State of the Art and Recent Advances in Immunoanalytical Systems. *Biosens. Bioelectron.* **2006**, *21*, 1424–1433.
- (4) Hock, B. Antibodies for Immunosensors a Review. *Anal. Chim. Acta* **1997**, *347*, 177–186.
- (5) Kurosawa, S.; Park, J.-W.; Aizawa, H.; Wakida, S.-I.; Tao, H.; Ishihara, K. Quartz Crystal Microbalance Immunosensors for Environmental Monitoring. *Biosens. Bioelectron.* **2006**, *22*, 473–481.
- (6) Butt, È.; Skla, P.; Raiteri, R.; Grattarola, M. Micromechanical Cantilever-Based Biosensors. *Sensors and actuators* **2001**, *79*, 115–126.
- (7) Guilbault, G. G.; Amia, F. Recent Developments in Piezoelectric Immunosensors\* A Review. *Analyst* **1994**, *11*, 2279–2282.
- (8) Abdulhalim, I.; Zourob, M.; Lakhtakia, A. Surface Plasmon Resonance for Biosensing: A Mini-Review. *Electromagnetics* **2008**, *28*, 214–242.
- (9) Lee, C.-S.; Kim, S. K.; Kim, M. Ion-Sensitive Field-Effect Transistor for Biological Sensing. *Sensors* **2009**, *9*, 7111–7131.
- (10) Liang, K.; Mu, W.; Huang, M.; Yu, Z.; Lai, Q. Interdigitated Conductometric Immunosensor for Determination of Interleukin-6 in Humans Based on Dendrimer G4 and Colloidal Gold Modified Composite Film. *Electroanalysis* **2006**, *18*, 1505–1510.
- (11) Yang, L.; Li, Y.; Erf, G. F. Interdigitated Array Microelectrode-Based Electrochemical Impedance Immunosensor for Detection of Escherichia Coli O157 : H7. *Anal. Chem.* **2004**, *76*, 1107–1113.
- (12) Hays, H. C. W.; Millner, P. a.; Prodromidis, M. I. Development of Capacitance Based Immunosensors on Mixed Self-Assembled Monolayers. *Sensors Actuators B Chem.* **2006**, *114*, 1064–1070.
- (13) Wan, Y.; Su, Y.; Zhu, X.; Liu, G.; Fan, C. Development of Electrochemical Immunosensors towards Point of Care Diagnostics. *Biosens. Bioelectron.* **2013**, *47*, 1–11.

- 1  
2  
3  
4  
5  
6  
7  
8  
9  
10  
11  
12  
13  
14  
15  
16  
17  
18  
19  
20  
21  
22  
23  
24  
25  
26  
27  
28  
29  
30  
31  
32  
33  
34  
35  
36  
37  
38  
39  
40  
41  
42  
43  
44  
45  
46  
47  
48  
49  
50  
51  
52  
53  
54  
55  
56  
57  
58  
59  
60
- (14) Casal, P.; Wen, X.; Gupta, S.; Nicholson, T.; Wang, Y.; Theiss, A.; Bhushan, B.; Brillson, L.; Lu, W.; Lee, S. C. ImmunofET Feasibility in Physiological Salt Environments. *Philos. Trans. A. Math. Phys. Eng. Sci.* **2012**, *370*, 2474–2488.
- (15) Palazzo, G.; De Tullio, D.; Magliulo, M.; Mallardi, A.; Intranuovo, F.; Mulla, M. Y.; Favia, P.; Vikholm-Lundin, I.; Torsi, L. Detection Beyond Debye's Length with an Electrolyte-Gated Organic Field-Effect Transistor. *Adv. Mater.* **2014**, 1–6.
- (16) Sheehan, a. D.; Quinn, J.; Daly, S.; Dillon, P.; O'Kennedy, R. The Development of Novel Miniaturized Immuno-Sensing Devices: A Review of a Small Technology with a Large Future. *Anal. Lett.* **2003**, *36*, 511–537.
- (17) Campana, A.; Cramer, T.; Simon, D. T.; Berggren, M.; Biscarini, F. Electrocardiographic Recording with Conformable Organic Electrochemical Transistor Fabricated on Resorbable Bioscaffold. *Adv. Mater.* **2014**, *26*, 3874–3878.
- (18) Cramer, T.; Chelli, B.; Murgia, M.; Barbalinardo, M.; Bystrenova, E.; de Leeuw, D. M.; Biscarini, F. Organic Ultra-Thin Film Transistors with a Liquid Gate for Extracellular Stimulation and Recording of Electric Activity of Stem Cell-Derived Neuronal Networks. *Phys. Chem. Chem. Phys.* **2013**, *15*, 3897–3905.
- (19) Khodagholy, D.; Doublet, T.; Quilichini, P.; Gurfinkel, M.; Leleux, P.; Ghestem, A.; Ismailova, E.; Hervé, T.; Sanaur, S.; Bernard, C.; *et al.* In Vivo Recordings of Brain Activity Using Organic Transistors. *Nat. Commun.* **2013**, *4*, 1–7.
- (20) Cramer, T.; Kyndiah, a.; Murgia, M.; Leonardi, F.; Casalini, S.; Biscarini, F. Double Layer Capacitance Measured by Organic Field Effect Transistor Operated in Water. *Appl. Phys. Lett.* **2012**, *100*, 143302.
- (21) Cramer, T.; Campana, A.; Leonardi, F.; Casalini, S.; Kyndiah, A.; Murgia, M.; Biscarini, F. Water-Gated Organic Field Effect Transistors – Opportunities for Biochemical Sensing and Extracellular Signal Transduction. *J. Mater. Chem. B* **2013**, *1*, 3728–3741.
- (22) Casalini, S.; Leonardi, F.; Cramer, T.; Biscarini, F. Organic Field-Effect Transistor for Label-Free Dopamine Sensing. *Org. Electron.* **2013**, *14*, 156–163.
- (23) Kergoat, L.; Piro, B.; Berggren, M.; Pham, M.-C.; Yassar, A.; Horowitz, G. DNA Detection with a Water-Gated Organic Field-Effect Transistor. *Org. Electron.* **2012**, *13*, 1–6.
- (24) Buth, F.; Kumar, D.; Stutzmann, M.; Garrido, J. a. Electrolyte-Gated Organic Field-Effect Transistors for Sensing Applications. *Appl. Phys. Lett.* **2011**, *98*, 153302.
- (25) Buth, F.; Donner, A.; Sachsenhauser, M.; Stutzmann, M.; Garrido, J. a. Biofunctional Electrolyte-Gated Organic Field-Effect Transistors. *Adv. Mater.* **2012**, *24*, 4511–4517.

- 1  
2  
3  
4 (26) Magliulo, M.; Mallardi, A.; Mulla, M. Y.; Cotrone, S.; Pistillo, B. R.; Favia, P.; Vikholm-  
5 Lundin, I.; Palazzo, G.; Torsi, L. Electrolyte-Gated Organic Field-Effect Transistor  
6 Sensors Based on Supported Biotinylated Phospholipid Bilayer. *Adv. Mater.* **2012**, 1–5.  
7  
8 (27) Evans, E.; Ritchie, K. Dynamic Strength of Molecular Adhesion Bonds. *Biophys. J.* **1997**,  
9 72, 1541–1555.  
10  
11 (28) Merkel, R.; Nassoy, P.; Leung, A.; Ritchie, K.; Evans, E. Energy Landscapes of Receptor-  
12 Ligand Bonds Explored with Dynamic Force Spectroscopy. *Nature* **1999**, 397, 50–53.  
13  
14 (29) Medalsy, I. D.; Müller, D. J. Nanomechanical Properties of Proteins and Membranes  
15 Depend on Loading Rate and Electrostatic Interactions. *ACS Nano* **2013**, 7, 2642–2650.  
16  
17 (30) Florin, E. L.; Moy, V. T.; Gaub, H. E. Adhesion Forces between Individual Ligand-  
18 Receptor Pairs. *Science (80-. )*. **1994**, 264, 415–417.  
19  
20 (31) Moy, V. T.; Florin, E. L.; Gaub, H. E. Intermolecular Forces and Energies between  
21 Ligands and Receptors. *Science* **1994**, 266, 257–259.  
22  
23 (32) Hinterdorfer, P.; Baumgartner, W.; Gruber, H. J.; Schilcher, K.; Schindler, H. Detection  
24 and Localization of Individual Antibody-Antigen Recognition Events by Atomic Force  
25 Microscopy. *Proc. Natl. Acad. Sci.* **1996**, 93, 3477–3481.  
26  
27 (33) Brogan, K. L.; Schoenfish, M. H. Influence of Antibody Immobilization Strategy on  
28 Molecular Recognition Force Microscopy Measurements. *Langmuir* **2005**, 21, 3054–3060.  
29  
30 (34) Carrion-Vazquez, M.; Oberhauser, A. F.; Fowler, S. B.; Marszalek, P. E.; Broedel, S. E.;  
31 Clarke, J.; Fernandez, J. M. Mechanical and Chemical Unfolding of a Single Protein: A  
32 Comparison. *Proc. Natl. Acad. Sci.* **1999**, 96, 3694–3699.  
33  
34 (35) Rief, M.; Gautel, M.; Oesterhelt, F.; Fernandez, J. M.; Gaub, H. E. Reversible Unfolding  
35 of Individual Titin Immunoglobulin Domains by AFM. *Science (80-. )*. **1997**, 276, 1109–  
36 1112.  
37  
38 (36) Tromas, C.; Rojo, J.; de la Fuente, J. M.; Barrientos, A. G.; García, R.; Penadés, S.  
39 Adhesion Forces between LewisX Determinant Antigens as Measured by Atomic Force  
40 Microscopy. *Angew. Chemie Int. Ed.* **2001**, 40, 3052–3055.  
41  
42 (37) Müller, D. J.; Dufrière, Y. F. Force Nanoscopy of Living Cells. *Curr. Biol.* **2011**, 21,  
43 R212–R216.  
44  
45 (38) Ledebøer, A.; Brevé, J. J. P.; Poole, S.; Tilders, F. J. H.; Dam, A. V. A. N. Interleukin-10,  
46 Interleukin-4 and Transforming Growth Factor-Beta Differentially Regulate  
47 Lipopolysaccharide-Induced Production of pro-Inflammatory Cytokines and Nitric Oxide  
48 in Co-Cultures of Rat Astroglial and Microglial Cells. *Glia* **2000**, 30, 134–142.  
49  
50  
51  
52  
53  
54  
55  
56  
57  
58  
59  
60

- 1  
2  
3  
4  
5  
6  
7  
8  
9  
10  
11  
12  
13  
14  
15  
16  
17  
18  
19  
20  
21  
22  
23  
24  
25  
26  
27  
28  
29  
30  
31  
32  
33  
34  
35  
36  
37  
38  
39  
40  
41  
42  
43  
44  
45  
46  
47  
48  
49  
50  
51  
52  
53  
54  
55  
56  
57  
58  
59  
60
- (39) Wirjatijasa, F.; Dehghani, F.; Blaheta, R. a; Korf, H.-W.; Hailer, N. P. Interleukin-4, Interleukin-10, and Interleukin-1-Receptor Antagonist but Not Transforming Growth Factor-Beta Induce Ramification and Reduce Adhesion Molecule Expression of Rat Microglial Cells. *J. Neurosci. Res.* **2002**, *68*, 579–587.
- (40) Yang, M.-S.; Park, E. J.; Sohn, S.; Kwon, H. J.; Shin, W.-H.; Pyo, H. K.; Jin, B.; Choi, K. S.; Jou, I.; Joe, E.-H. Interleukin-13 and -4 Induce Death of Activated Microglia. *Glia* **2002**, *38*, 273–280.
- (41) Lee, S. I.; Jeong, S. R.; Kang, Y. M.; Han, D. H.; Jin, B. K.; Namgung, U.; Kim, B. G. Endogenous Expression of Interleukin-4 Regulates Macrophage Activation and Confines Cavity Formation after Traumatic Spinal Cord Injury. *J. Neurosci. Res.* **2010**, *88*, 2409–2419.
- (42) Betancor, L.; López-Gallego, F.; Hidalgo, A.; Alonso-Morales, N.; Mateo, G. D.-O. C.; Fernández-Lafuente, R.; Guisán, J. M. Different Mechanisms of Protein Immobilization on Glutaraldehyde Activated Supports: Effect of Support Activation and Immobilization Conditions. *Enzyme Microb. Technol.* **2006**, *39*, 877–882.
- (43) Walt, D. R.; Agayn, V. I. The Chemistry of Enzyme and Protein Immobilization with Glutaraldehyde. *Trends Anal. Chem.* **1994**, *13*, 425–430.
- (44) Yang, Z.; Zhao, Y.-P. Adsorption of His-Tagged Peptide to Ni, Cu and Au (100) Surfaces: Molecular Dynamics Simulation. *Eng. Anal. Bound. Elem.* **2007**, *31*, 402–409.
- (45) Soong, R. K.; Stelick, S. J.; Bachand, G. D.; Montemagno, C. D. Evaluating Adhesion Strength of Biological Molecules to Nanofabricated Substrates. In *INTERNATIONAL CONFERENCE ON MODELING AND SIMULATION OF MICROSYSTEMS*; 1999; pp. 95–98.
- (46) Bachand, G. D.; Montemagno, C. D. Constructing Organic / Inorganic NEMS Devices Powered by Biomolecular Motors. *Biomed. Microdevices* **2000**, *2:3*, 179–184.
- (47) Baio, J. E.; Cheng, F.; Ratner, D. M.; Stayton, P. S.; Castner, D. G. Probing Orientation of Immobilized Humanized Anti-Lysozyme Variable Fragment by Time-of-Flight Secondary-Ion Mass Spectrometry. *J. Biomed. Mater. Res. A* **2011**, 1–7.
- (48) Trilling, A. K.; Beekwilder, J.; Zuilhof, H. Antibody Orientation on Biosensor Surfaces: A Minireview. *Analyst* **2013**, *138*, 1619–1627.
- (49) Bae, Y. M.; Oh, B.-K.; Lee, W.; Lee, W. H.; Choi, J.-W. Study on Orientation of Immunoglobulin G on Protein G Layer. *Biosens. Bioelectron.* **2005**, *21*, 103–110.
- (50) Song, H. Y.; Zhou, X.; Hobley, J.; Su, X. Comparative Study of Random and Oriented Antibody Immobilization as Measured by Dual Polarization Interferometry and Surface Plasmon Resonance Spectroscopy. *Langmuir* **2012**, *28*, 997–1004.

- 1  
2  
3  
4 (51) Mark, L. W.; Smith, D. A. Complex Chemical Force Titration Behavior of Amine-  
5 Terminated Self-Assembled Monolayers. *Langmuir* **2001**, *17*, 1126–1131.  
6  
7 (52) San Paulo, A.; García, R. Attractive and Repulsive Tip-Sample Interaction Regimes in  
8 Tapping-Mode Atomic Force Microscopy. *Phys. Rev. B* **1999**, *60*, 4961–4967.  
9  
10 (53) Zhao, X.; Yaseen, M.; Pan, F.; Lu, J. R.; Street, M.; Sheffield, S. *Protein and Interfaces*  
11 *III. State of the Art*; 2012; pp. 543–574.  
12  
13 (54) Ido, S.; Kimiya, H.; Kobayashi, K.; Kominami, H.; Matsushige, K.; Yamada, H.  
14 Immunoactive Two-Dimensional Self-Assembly of Monoclonal Antibodies in Aqueous  
15 Solution Revealed by Atomic Force Microscopy. *Nat. Mater.* **2014**, *13*, 264–270.  
16  
17 (55) Press, W. H.; Teukolsky, S. A.; Vetterling, W. T.; Flannery, B. P. *Numerical Recipes, The*  
18 *Art of Scientific Computing*; 2007.  
19  
20 (56) Abramowitz, M.; Stegun, I. A. *Handbook of Mathematical Functions with Formulas,*  
21 *Graphs, and Mathematical Tables*; 1972.  
22  
23 (57) Biscarini, F.; Zamboni, R.; Samorì, P.; Ostoja, P.; Taliani, C. Growth of Conjugated  
24 Oligomer Thin Films Studied by Atomic-Force Microscopy. *Phys. Rev. B* **1995**, *52*,  
25 14868–14877.  
26  
27 (58) Schwesinger, F.; Ros, R.; Strunz, T.; Anselmetti, D.; Güntherodt, H.-J.; Honegger, A.;  
28 Jermutus, L.; Tiefenauer, L.; Plückthun, A. Unbinding Forces of Single Antibody-Antigen  
29 Complexes Correlate with Their Thermal Dissociation Rates. *Proc. Natl. Acad. Sci.* **2000**,  
30 *97*, 9972–9977.  
31  
32 (59) Brogan, K. L.; Shin, J. H.; Schoenfisch, M. H. Influence of Surfactants and Antibody  
33 Immobilization Strategy on Reducing Nonspecific Protein Interactions for Molecular  
34 Recognition Force Microscopy. *Langmuir* **2004**, *20*, 9729–9735.  
35  
36 (60) Berquand, A.; Xia, N.; Castner, D. G.; Clare, B. H.; Abbott, N. L.; Dupres, V.;  
37 Adriaensens, Y.; Dufrene, Y. F. Antigen Binding Forces of Single Antilysozyme Fv  
38 Fragments Explored by Atomic Force Microscopy. *Langmuir* **2005**, *21*, 5517–5523.  
39  
40 (61) Kienberger, F.; Kada, G.; Mueller, H.; Hinterdorfer, P. Single Molecule Studies of  
41 Antibody-Antigen Interaction Strength versus Intra-Molecular Antigen Stability. *J Mol*  
42 *Biol* **2005**, *347*, 597–606.  
43  
44 (62) Van Es, M. H.; Tang, J.; Preiner, J.; Hinterdorfer, P.; Oosterkamp, T. H. Single Molecule  
45 Binding Dynamics Measured with Atomic Force Microscopy. *Ultramicroscopy* **2014**, *140*,  
46 32–36.  
47  
48  
49  
50  
51  
52  
53  
54  
55  
56  
57  
58  
59  
60

- 1  
2  
3  
4  
5  
6  
7  
8  
9  
10  
11  
12  
13  
14  
15  
16  
17  
18  
19  
20  
21  
22  
23  
24  
25  
26  
27  
28  
29  
30  
31  
32  
33  
34  
35  
36  
37  
38  
39  
40  
41  
42  
43  
44  
45  
46  
47  
48  
49  
50  
51  
52  
53  
54  
55  
56  
57  
58  
59  
60
- (63) Bizzarri, A. R.; Cannistraro, S. The Application of Atomic Force Spectroscopy to the Study of Biological Complexes Undergoing a Biorecognition Process. *Chem Soc Rev* **2010**, *39*, 734–749.
- (64) Bonanni, B.; Bizzarri, A. R.; Cannistraro, S. Optimized Biorecognition of Cytochrome c 551 and Azurin Immobilized on Thiol-Terminated Monolayers Assembled on Au ( 111 ) Substrates. *J. Phys. Chem. B* **2006**, *551*, 14574–14580.
- (65) Bonanni, B.; Kamruzzahan, A. S. M.; Bizzarri, A. R.; Rankl, C.; Gruber, H. J.; Hinterdorfer, P. Single Molecule Recognition between Cytochrome C 551 and Gold-Immobilized Azurin by Force Spectroscopy. *Biophys. J.* **2005**, *89*, 2783–2791.
- (66) Eyring, H. The Activated Complex in Chemical Reactions. *J. Chem. Phys.* **1935**, *3*, 107–115.
- (67) Oesterhelt, F.; Rief, M.; Gaub, H. E. Single Molecule Force Spectroscopy by AFM Indicates Helical Structure of Poly ( Ethylene-Glycol ) in Water. *New J. Phys.* **1999**, *1*, 6.1–6.11.
- (68) Walczak, M.; Popenoe, D. D.; Deinhammer, R. S.; Lamp, B. D.; Chung, C.; Porter, M. D. Reductive Desorption of Alkanethiolate Monolayers at Gold: A Measure of Surface Coverage. *Langmuir* **1991**, 2687–2693.
- (69) Widrig, A.; Porter, M. D. The Electrochemical Desorption of N-Alkanethiol from Polycrystalline Au and Ag Electrodes Monolayers. *J. Electroanal. Chem.* **1991**, *310*, 335–359.
- (70) Campana, A.; Cramer, T.; Greco, P.; Foschi, G.; Murgia, M.; Biscarini, F. Facile Maskless Fabrication of Organic Field Effect Transistors on Biodegradable Substrates. *Appl. Phys. Lett.* **2013**, *103*, 073302.
- (71) Casalini, S.; Shehu, A.; Destri, S.; Porzio, W.; Pasini, M. C.; Vignali, F.; Borgatti, F.; Albonetti, C.; Leonardi, F.; Biscarini, F. Organic Field-Effect Transistors as New Paradigm for Large-Area Molecular Junctions. *Org. Electron.* **2012**, *13*, 789–795.
- (72) Garcia, R.; San Paulo, A. Attractive and Repulsive Tip-Sample Interaction Regimes in Tapping-Mode Atomic Force Microscopy. *Phys. Rev. B* **1999**, *60*, 4961–4967.
- (73) Herruzo, E. T.; Garcia, R. Frequency Response of an Atomic Force Microscope in Liquids and Air: Magnetic versus Acoustic Excitation. *Appl. Phys. Lett.* **2007**, *91*, 143113.
- (74) Butt, H.-J.; Jaschke, M. Calculation of Thermal Noise in Atomic Force Microscopy. *Nanotechnology* **1995**, *6*, 1–7.

1  
2  
3  
4  
5  
6  
7  
8  
9  
10  
11  
12  
13  
14  
15  
16  
17  
18  
19  
20  
21  
22  
23  
24  
25  
26  
27  
28  
29  
30  
31  
32  
33  
34  
35  
36  
37  
38  
39  
40  
41  
42  
43  
44  
45  
46  
47  
48  
49  
50  
51  
52  
53  
54  
55  
56  
57  
58  
59  
60

## SUPPORTING INFO

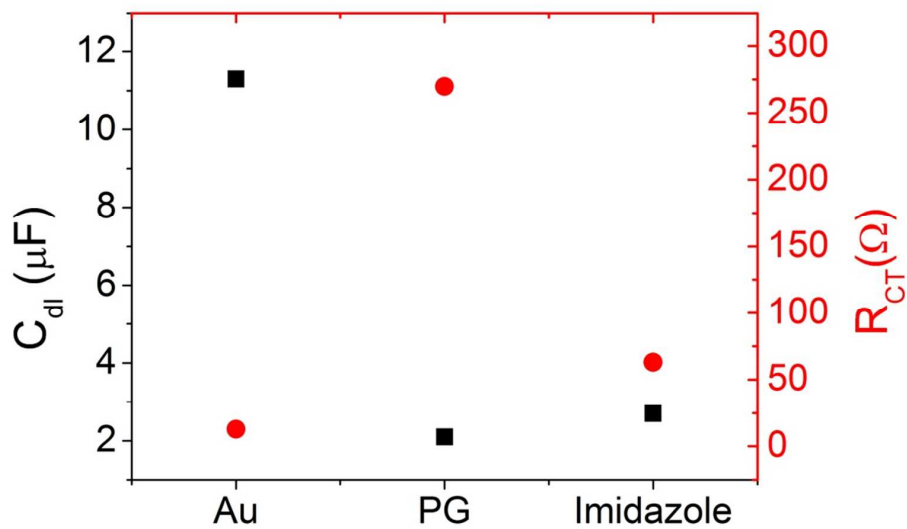


**Figure S1** Overlay of the double-layer capacitance and charge transfer resistance for bare Au, PG adsorbed on it and imidazole elution.

Electrode modifiers	$C_{dl}$ ( $\mu\text{F}$ )	$R_{CT}$ ( $\text{k}\Omega$ )
$\text{HSC}_6\text{NH}_2$	$1.3(\pm 0.1)$	$0.7(\pm 0.1)$
$\text{HSC}_6\text{NH}_2 + \text{Anti-IL4}$	$0.56(\pm 0.07)$	$2.3 (\pm 0.1)$
PG	$1.14(\pm 0.02)$	$3.1(\pm 0.1)$
PG + Anti-IL4	$1.22(\pm 0.02)$	$4.3(\pm 0.1)$

**Table S1**  $C_{dl}$  and  $R_{CT}$  values are listed for the two functionalization protocols.

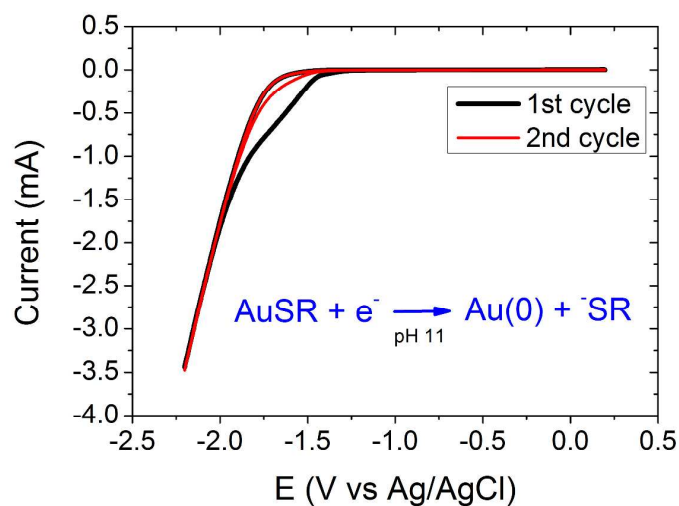


**Figure S2** Reductive electrochemical desorption of the bio-material chemically adsorbed on polycrystalline Au. First scan (black line) and second one (red line) are overlaid.

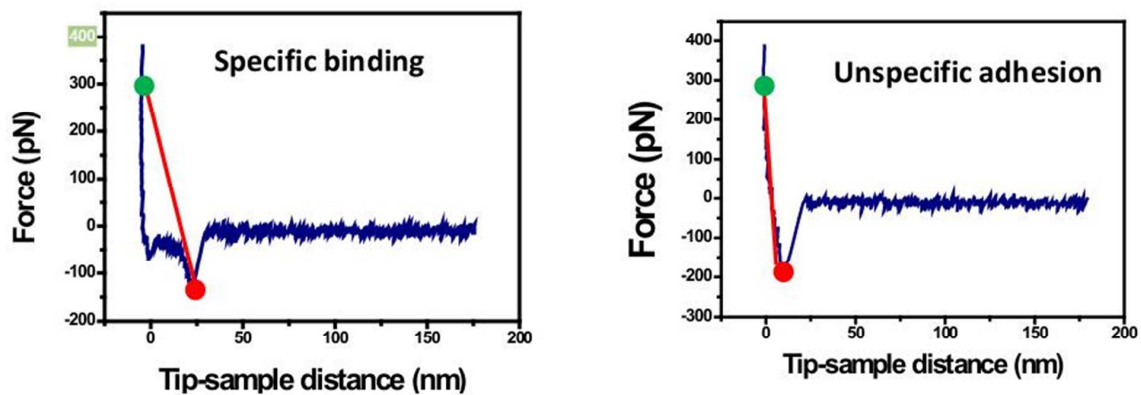


**Figure S4** Scheme of the algorithm used to discriminate between specific recognition event, and unspecific adhesion.

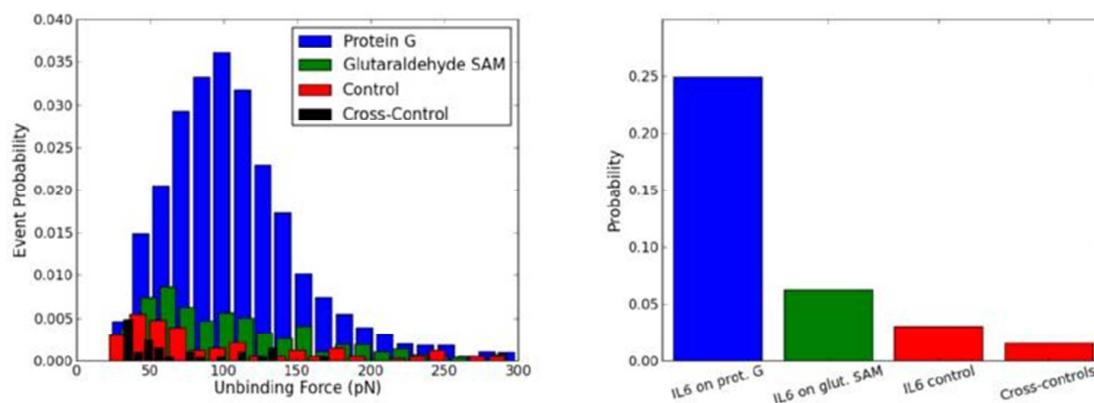


**Figure S5** (a) Histogram and (b) bar-plot of the probability percentage for specific, aspecific immobilization, control experiments for IL6 antibody-antigen recognition.

1  
2  
3  
4  
5  
6  
7  
8  
9  
10  
11  
12  
13  
14  
15  
16  
17  
18  
19  
20  
21  
22  
23  
24  
25  
26  
27  
28  
29  
30  
31  
32  
33  
34  
35  
36  
37  
38  
39  
40  
41  
42  
43  
44  
45  
46  
47  
48  
49  
50  
51  
52  
53  
54  
55  
56  
57  
58  
59  
60

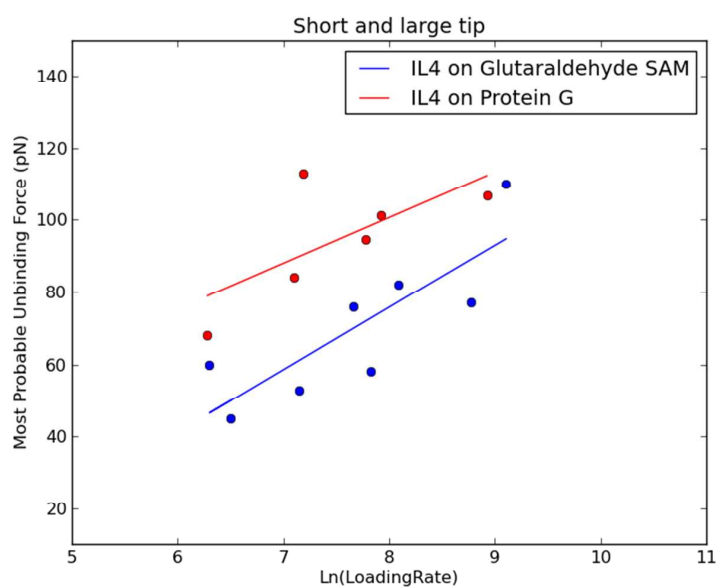


**Figure S6** Most probable unbinding force vs loading rate for (a) aspecific and (b) specific functionalization: